

Time stamps of vertical phase mixing in the Galactic disk from LAMOST-Gaia stars

HAI-JUN TIAN,^{1,2,3} CHAO LIU,⁴ YUE WU,⁴ MAO-SHENG XIANG,⁴ AND YONG ZHANG⁵

¹*China Three Gorges University, Yichang 443002, China*

²*Center of Astronomy and Space Science Research, China Three Gorges University, Yichang 443002, China*

³*Max Planck Institute for Astronomy, Königstuhl 17, D-69117 Heidelberg, Germany*

⁴*Key Lab for Optical Astronomy, National Astronomical Observatories, Chinese Academy of Sciences, Beijing 100012, China*

⁵*Nanjing Institute of Astronomical Optics & Technology, National Astronomical Observatories, Chinese Academy of Sciences, Nanjing 210042, China*

(Received Jul. 31st, 2018; Revised Aug. 2nd, 2018; Accepted Sep. 18th, 2018)

Submitted to ApJL

ABSTRACT

The perturbation mechanism of the Galactic disk has puzzled us for a long time. The imprints from perturbations provide important diagnostics on the disk formation and evolution. Here we try to constrain when the vertical perturbation took place in the disk by tracking the phase mixing history. Firstly, we clearly depict the spiral structures of radial (v_R) and azimuthal (v_ϕ) velocities in the phase space of the vertical position and velocity (z - v_z) with 723,871 LAMOST-Gaia combined stars. Then, we investigate the variation of the spirals with stellar age (τ) by dividing the sample into seven stellar age bins. Finally, we find that the spirals explicitly exist in all the bins, even in the bin of $\tau < 0.5$ Gyr, except for the bin of $\tau > 6.0$ Gyr. This constrains the vertical perturbation probably starting no later than 0.5 Gyr ago. But we can not rule out whether the young stars ($\tau < 0.5$ Gyr) inherit the oscillations from the perturbed ISM where they born from. This study provides some important observational evidences to understand the disk perturbation mechanisms, even the formation and evolution of our Galaxy.

Keywords: Galaxy: kinematics and dynamics - Galaxy: disk - Galaxy: structure

1. INTRODUCTION

The Galactic disk has been revealed to suffer from perturbations, which have imprints in both the stellar density (Widrow et al. 2012; Gómez et al. 2013; Xu et al. 2015; Wang et al. 2018b; Xiang et al. 2018) and kinematics (Siebert et al. 2011; Tian et al. 2015, 2017; Wang et al. 2018a; Gaia Collaboration: Katz et al. 2018). The perturbations in the plane are typically explained in terms of the influence of the non-axisymmetric components of the Galaxy, e.g. the rotating bar (Monari et al. 2013; Bovy et al. 2015), the spiral arms (Siebert et al. 2012; Faure et al. 2014; Kawata et al. 2014) or both (Quillen et al. 2011; Grand et al. 2015; Tian et al. 2017). The vertical perturbations are usually thought to be excited by minor mergers, such as the passage of

the Sagittarius dwarf galaxy through the Galactic disc (Gómez et al. 2013). However, some proofs were found from simulations that the rotating bar and the spiral arms can also give rise to significant vertical influence (Monari et al. 2013; Faure et al. 2014; Debattista 2014). Tian et al. (2015) showed that the asymmetric motion may be related to the age of the stars, i.e. the younger populations show larger peculiar velocity in both radial and vertical directions than the old populations. Also the non-zero radial flow can be simply explained with the projection effect in the elliptical stellar orbits (Tian et al. 2017).

More recently, Antoja (2018, hereafter A18) found, from Gaia DR2 stars, that the disk is full of substructures in the phase space. It indicates that the Galactic disk is currently undergoing the phase mixing, and unveils that the Galactic disk has experienced vertical perturbation. In the phase space of z - v_z , the stars take on an impressive curled spiral-shaped distribution

in the radial velocity (v_R) and the azimuthal velocity (v_ϕ). Based on the impulse-approximation, Binney & Schönrich (2018) built a simple model to explain the origin of the phase-plane spiral. The key factors that lead to a spiral are: that the vertical frequency Ω_z depends on angular momentum not only in J_z but also in J_ϕ , and that the stellar vertical oscillations should be in anharmonic state, which could be perturbed by an intruder, such as a dwarf galaxy or a pure dark-matter structure. Laporte et al. (2018) used a set of numerical N-body simulations, in which a Sgittarius-like dSph (Sgr) hits a Milky Way-like host, to follow the orbit of Sgr from the first pericentric passage to the present-day, and illustrate the evolution of the phase-space spirals in the last Gyr.

In this study, we propose to constrain when the perturbation took place in the disk, by tracking the phase mixing history with different stellar population. The cornerstone Gaia has already measured precise proper motions and distances for more than 1.3 billion stars. And the LAMOST survey (Zhao et al. 2012; Liu et al. 2014) has collected more than 9 million stellar spectra, and built the largest stellar atmospheric parameter library in the world. The combination of the Gaia and LAMOST provides us an unprecedented sample to track the history of the phase mixing in a large spatial volume.

This Letter is organized as follows. In Section 2, the sample selection is briefly described. The results and discussion are presented in Section 3. Finally, we conclude this work in Section 4.

Throughout the paper, we adopt the solar motion as $(U_\odot, V_\odot, W_\odot) = (9.58, 10.52, 7.01) \text{ km s}^{-1}$ (Tian et al. 2015), the circular speed of the local standard of rest (LSR) as $v_0 = 238 \text{ km s}^{-1}$ (Schönrich 2012), and the solar Galactocentric radius and vertical positions as $(R_0, z_0) = (8.27, 0.02) \text{ kpc}$ (Schönrich et al. 2010; Schönrich 2012).

2. THE SAMPLE SELECTION

In order to build the sample containing stellar astrophysical parameters and precise kinematical informations, we combine the data from the two surveys: the LAMOST spectroscopic survey (Zhao et al. 2012; Cui et al. 2012), and Gaia (Gaia Collaboration et al. 2016) survey.

LAMOST is a quasi-meridian reflecting Schmidt telescope with an effective aperture of about 4 m and a field of view of 5° . The LAMOST Survey has internally delivered the fifth data release (DR5), which contains 9,017,844 spectra with a resolution of ~ 1800 covering a wavelength range of $3800 \text{ \AA} \lesssim \lambda \lesssim 9000 \text{ \AA}$. In the catalog, the LAMOST stellar parameter pipeline - LASP has de-

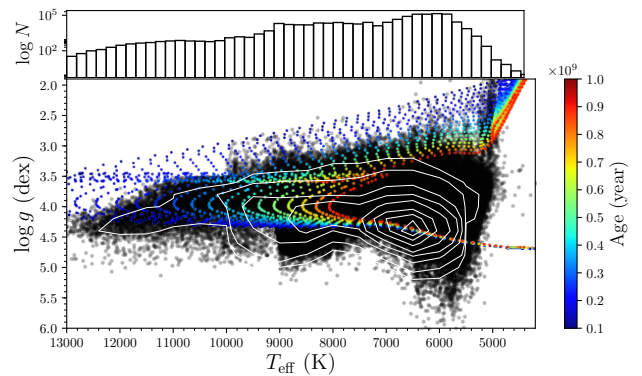


Figure 1. The sample distribution in the $T_{\text{eff}}\text{-log } g$ panel. The black points display the 723,871 LAMOST-Gaia stars used in this work. The isochrones are color-coded with stellar ages, to demonstrate the distribution of young stellar population ($\tau < 1.0 \text{ Gyr}$). The histogram in the top sub-panel presents the logarithmic number of stars in T_{eff} bins. The contours indicate the normalized number density of stars with different levels of 0.003, 0.01, 0.05, 0.1, 0.2, 0.4, 0.6, and 0.8 (the highest density is normalized to 1).

rived those stellar astrophysical parameters (T_{eff} , $\log g$, and $[\text{Fe}/\text{H}]$) as well as the line-of-sight velocities for 5,475,513 stars (Wu et al. 2011a, 2014). LAMOST radial velocities are as precise as about 5 km s^{-1} , but with a systematical under-estimation of $\sim 5.7 \text{ km s}^{-1}$ (Tian et al. 2015).

Gaia DR2 (Gaia Collaboration: Brown et al. 2018) includes more than 1.3 billion stars in the Milk Way with G-band magnitude brighter than ~ 20.7 , which were measured the precise position, proper motions and parallaxes. Bailer-Jones et al. (2018) calculated the distances and the asymmetric uncertainties for the stars from the parallaxes in the Gaia DR2.

Cross-matching the LAMOST DR5 with Gaia DR2, and removing the duplicated observations, we obtained 4,130,116 stars which not only have the LAMOST astrophysical parameters and line-of-sight velocity, but also have Gaia distances and proper motions. This provides us an unprecedented sample to track the stellar phase mixing history.

In order to obtain the stellar ages, we further cross-matched the LAMOST-Gaia sample with an updated-version of the age catalog from Xiang et al. (2017). The catalog of Xiang et al. (2017) contains stellar ages and masses of 0.93 million Galactic-disk main-sequence turnoff (MSTO) and sub-giant stars from LAMOST DR4. The ages are determined by matching with stellar isochrones using a Bayesian algorithm, utilizing effective temperature T_{eff} , absolute magnitude M_V , metallicity $[\text{Fe}/\text{H}]$, and α -element to iron abundance ratio $[\alpha/\text{Fe}]$ deduced from the LAMOST spectra. In this work, the

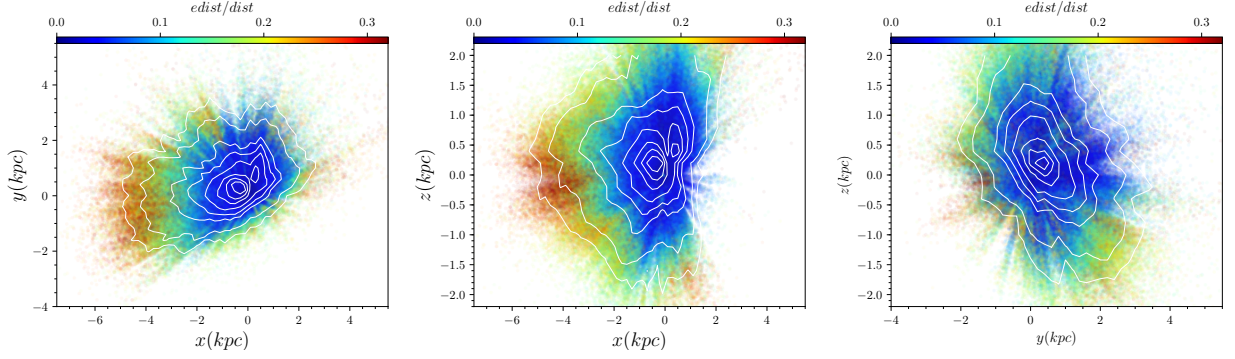


Figure 2. The spatial distribution of the sample in the Cartesian coordinates. The left (x-y), middle (x-z), and right (y-z) panels show the projected stellar distributions, respectively. The color bars indicate the relative distance errors measured from Gaia DR2 parallaxes by Bailer-Jones et al. (2018). In total, more than 95% stars have relative distance errors ($edist/dist$) of $< 20\%$. The contours have the same meaning as Fig. 1.

stellar ages are re-calculated with the same procedure of Xiang et al. (2017), but using the absolute magnitudes deduced from Gaia DR2 parallaxes. To avoid strong bias in the deduced absolute magnitudes (thus ages) from the Gaia parallaxes, we restrict our sample stars with relative parallax errors smaller than 20%. The precision of the newly estimated ages are significantly improved relative to that of Xiang et al. (2017). The whole sample has a median error of 22% for the age estimates, and about 70% of the stars are older than 2 Gyr.

We notice that Xiang et al. (2017) discard all stars with $T_{\text{eff}} > 10000$ K, because the atmospheric parameters of those hot stars given by LSP3 (Xiang et al. 2015) have poor precision. The temperature cut discards most stars younger than 0.5 Gyr, which are extremely important for the purpose of current paper.

To select younger stars, we pre-select A-type star candidates according to the following empirical criteria (Liu et al. 2015),

- $EW_{\text{Fe}} < 0.6$ & $EW_{H\gamma} < 6$ & $EW_{\text{Fe}} < (0.6 - 0.2)/(6 - 13) * (EW_{H\gamma} - 6) + 0.6$ & $EW_{H\gamma} \geq 6$,
- $EW_{G4300} < 0.2$ & $EW_{H\gamma} < 6$ & $G < (0.2 + 2.5)/(6 - 13.2) * (EW_{H\gamma} - 6) + 0.2$ & $EW_{H\gamma} \geq 6$ & $EW_{\text{Mg}} < (-0.2 - 1.2)/(-5 - 16.5) * (EW_{H\gamma} + 5) - 0.2$,

where $EW_{H\gamma}$ and EW_{G4300} are equivalent widths (EWs) of H_γ and G-band (defined in Liu et al. (2015)). EW_{Fe} is the averaged EW of nine Fe lines located at 4383, 4531, 4668, 5015, 5270, 5335, 5406, 5709 and 5782 Å, EW_{Mg} is the averaged EW of three Lick indices, i.e. Mg I, Mg II and Mg_b (Worthey et al. 1994).

Then we derive the atmospheric parameters for the A-type star candidates by adopting ULYSS package (Wu et al. 2011b), and estimate the age for each star with the method in Xiang et al. (2017). The A-type stars used in this work are further purified with the following criteria:

- $T_{\text{eff}} > 7500$ K,
- $\log g > 3.5$,
- $\text{SNR} > 30$ in g-band

To get a sample with good age estimation, we discard stars with relative age error of $> 33\%$. Finally, we obtain a sample of 723,871 LAMOST-Gaia stars, shown as the black dots in Fig. 1. The color-coded isochrones with stellar ages mainly display the distribution of young stars ($\tau < 1.0$ Gyr) in the $T_{\text{eff}}\text{-}\log g$ panel. The spatial distributions of the sample in the Cartesian coordinate system are displayed in Fig 2, each dot is color-coded with its relative distance error. In total, more than 95% stars have relative distance error of $< 20\%$.

3. RESULTS AND DISCUSSION

We divide the sample into seven stellar age (τ) bins from 0.2 Gyr to ~ 10.0 Gyr, to investigate the spiral patterns at different stellar ages. Each stellar bin includes at least hundreds of thousands stars. The stellar number (N) of each bin is labeled in Fig. 3. To reduce the contamination of old stars, the youngest stellar bin with $\tau < 0.5$ Gyr only includes A-type stars.

3.1. The spirals in the LAMOST-Gaia Sample

We reproduce the spiral-shaped structures in the phase space of $z\text{-}v_z$ from the LAMOST-Gaia stars. Fig. 3 displays the $z\text{-}v_z$ phase-space spirals for $\langle v_R \rangle$ (the left column) and $\langle v_\phi \rangle$ (the right column) in different stellar age (τ) bins. The pixel has a size of $\Delta z = 0.01$ kpc and $\Delta v_z = 0.1$ km s^{-1} . The red and green curves in the minor sub-panels demonstrate the variations of $\langle v_R \rangle$ (or $\langle v_\phi \rangle$) with v_z in the two slices of $|z| < 0.1$ kpc and $|z + 0.1| < 0.1$ kpc, respectively. The yellow dashed lines mark the locations of $v_z = 15.0$ km s^{-1} and $v_z = -20.0$ km s^{-1} in the $\langle v_R \rangle$ sub-panel, and the locations of $v_z = 15.0$ km s^{-1} and $v_z = -25.0$ km s^{-1} in the $\langle v_\phi \rangle$ sub-panel.

They are roughly marked the locations of peaks in the $\langle v_R \rangle$ and $\langle v_\phi \rangle$ curves.

The spirals are significantly prominent for both $\langle v_R \rangle$ and $\langle v_\phi \rangle$, in particular in the middle three age bins, i.e. $1.0 \text{ Gyr} < \tau < 1.5 \text{ Gyr}$ (the 3rd row), $1.5 \text{ Gyr} < \tau < 2.5 \text{ Gyr}$ (the 4th row), and $2.5 \text{ Gyr} < \tau < 4.0 \text{ Gyr}$ (the 5th row). In the first and last second bins, i.e. $0.5 \text{ Gyr} < \tau < 1.0 \text{ Gyr}$ and $4.0 \text{ Gyr} < \tau < 6.0 \text{ Gyr}$, the spirals for both $\langle v_R \rangle$ and $\langle v_\phi \rangle$ are not clear, but still visible. The spirals in $\tau < 0.5 \text{ Gyr}$ are indistinguishable, since young stellar population is kinematically cold, the stars are confined to the centre of the z - v_z plane by the age-velocity dispersion relation. As the stellar age growing, however, the spirals become obscure in $\tau > 4.0 \text{ Gyr}$. When the stellar ages become larger than 6 Gyr , the spirals are almost disappeared. It indicates that the old stars, which are the kinematically hot stellar population, are not sensitive to the perturbation.

The red and green curves in the minor sub-panels show clear wiggles for both $\langle v_R \rangle$ and $\langle v_\phi \rangle$ in all the age bins, even in $\tau < 0.5 \text{ Gyr}$, but except for $\tau > 6.0 \text{ Gyr}$. And each wiggle has two pronounced peaks, which indicate two wraps in the z - v_z phase space. The interesting thing is that the peaks for $\langle v_R \rangle$ (or $\langle v_\phi \rangle$) are corresponding to the same v_z values in each age bin, and the peaks of $\langle v_R \rangle$ and $\langle v_\phi \rangle$ are roughly located in the same v_z values, except the 5 km s^{-1} difference at the negative v_z peak. These similar wiggles suggest that the spirals probably have the same origin.

3.2. A possible starting time of the phase mixing

We suppose that the on-going vertical phase mixing is sparked by an external perturbation, which not only impacts the stars, but also pulls the ISM coherently as it does the stars. If the perturbation on the ISM can be quickly dissipated, the newly born stars from the perturbed gas will not share the general oscillations. According to the age of the stellar population, in which the z - v_z phase spirals just appear, we could deduce the starting time of the phase mixing.

The most prominent feature in Fig. 3 is that the spirals are gradually apparent from $\tau < 0.5 \text{ Gyr}$, and then slowly disappearing until $\tau > 6.0 \text{ Gyr}$. This gradual changes of the spirals indicate that the different stellar populations have diverse sensitivity level to the perturbation. In addition, the oscillation signals have already existed in the stars with $\tau < 0.5 \text{ Gyr}$, as shown by the 1-D red and green curves in the minor sub-panels. This suggests that the vertical perturbation to the disk probably took place no later than 0.5 Gyr ago. This is consistent with the time predicted by A18, in which the authors claimed that the vertical phase mixing event

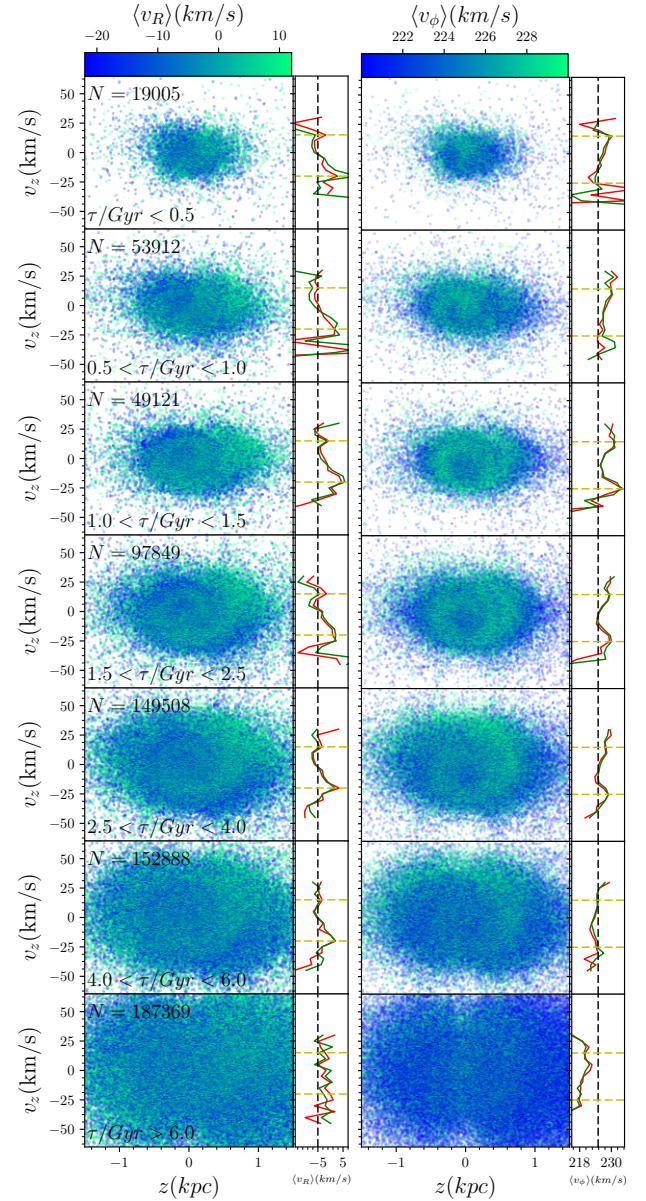


Figure 3. The spiral-shaped structures in the phase space of the vertical position and velocity (z - v_z) for the LAMOST-Gaia stars. The left panel is colored as a function of median v_R . The right panel is colored as a function of median v_ϕ . The pixel has a size of $\Delta z = 0.01 \text{ kpc}$ and $\Delta v_z = 0.1 \text{ km s}^{-1}$. Here N means the star number in each age bin. The red and green curves in the minor sub-panels demonstrate the variations of the $\langle v_R \rangle$ (or $\langle v_\phi \rangle$) with v_z in the two slices of $|z| < 0.1 \text{ kpc}$ and $|z + 0.1| < 0.1 \text{ kpc}$. The yellow dashed lines roughly indicate the locations of peaks in the $\langle v_R \rangle$ and $\langle v_\phi \rangle$ curves. The black dashed lines are just for reference, which are $\langle v_R \rangle = -5 \text{ km s}^{-1}$ and $\langle v_\phi \rangle = 225 \text{ km s}^{-1}$, respectively.

started about 500 Myr ago, with an uncertainty range of $[300, 900] \text{ Myr}$. This is a strong constraint on the perturbation time, but it is under the assumption that the young stars do not carry on the perturbation con-

tribution from the stimulated ISM where they are born from. It may be an ideal hypothesis. We will discuss more about it in Section 3.3.

3.3. Discussion

The explanations to the spirals in Section 3.2 are concise, but controversial. In this Section, we will discuss the issues in three aspects.

3.3.1. Clues of an early perturbation history

There are several clues, which favor that the vertical perturbation to the disk took place in $\tau < 0.5$ Gyr ago:

- Except for the old population in $\tau > 6.0$ Gyr, the spirals markedly existed in all the stellar age bins, especially in $\tau > 0.5$ Gyr. It suggests that stars in the disk probably have already been perturbed at least one time in the last 0.5 Gyr. This is a natural and straightforward explanation.
- The pictures of $\langle v_R \rangle$ and $\langle v_\phi \rangle$ in $\tau < 0.5$ Gyr look similar with the scenes presented by Laporte et al. (2018) in Fig. 5 and Fig. 6 at $t \sim 0$ Gyr, during which a Sagittarius-like dSph passed by the pericentre.
- The spirals in the different stellar bins look similar, and only take on two wraps, even in the old population in $4.0 < \tau < 6.0$ Gyr. The footprints of the dSph in the N-body simulation illustrate that the spirals can be formed in ~ 0.4 Gyr after the Sgr's last pericentric passage (see Fig. 5 and Fig. 6 of Laporte et al. (2018)). This also can be found in Fig. 7 of Binney & Schönrich (2018). If the perturbation took place $\tau > 0.5$ Gyr ago, the spirals perhaps will have more than two wraps, as showed in Fig. 9 of Darling & Widrow (2018).

3.3.2. Doubts on the perturbation time

Although some clues support an early perturbation history, but there still exist some debatable points:

- Is the perturbation on ISM able to dissipated in short time? This is an open question. If not, it suggests that for all the stars, whatever they were born before or after the perturbation took place, both v_R and v_ϕ will take on spiral patterns in the z - v_z phase space, or at least include the perturbation contribution in each stellar age bin. Strictly speaking, we can not rule out this case in this work.
- Stars possibly oscillate much more slowly than one usually image in the vertical direction. It suggests that the spirals possibly can not be formed within ~ 0.4 Gyr after the perturbation in reality.

- The perturbation time in different literatures are not converged well. Minchev et al. (2009) predicted that the Galactic disk was strongly perturbed ~ 1.9 Gyr ago, and associated the perturbation with Galactic bar formation. Monari et al. (2018) claimed that the disk experienced a vertical perturbation by the Sagittarius dwarf galaxy ~ 1.5 Gyr ago, and related it to the formation of the Coma Berenices moving group. A18 also inferred that the disk perturbation is caused by the passage of Sagittarius dwarf galaxy, but it occurred between 300 and 900 Myr ago. In this study, some clues suggest that the vertical perturbation in the disk possibly took place no later than 0.5 Gyr ago.

3.3.3. The comparison of stellar ages with others

The results in Section 3.2 might be affected by the bias of stellar ages. In order to investigate how the stellar ages are determined in this work, we compare our ages (τ_x) with the ages (τ_s) from Sanders & Das (2018) based on the 416,140 cross-matched stars. Fig. 4 display the histograms of age differences ($\Delta\tau = \tau_s - \tau_x$) in the seven stellar age bins adopted in Fig. 3.

As one can see, the two stellar ages are consistent within 1σ , except in the first two young stellar bins. However, τ_s is systematically larger than τ_x by 10% in $\tau > 1.0$ Gyr, and by $\sim 30\%$ in $\tau < 1.0$ Gyr. The systematical differences between τ_x and τ_s are probably due to the effect of $[\alpha/\text{Fe}]$. We used $[\alpha/\text{Fe}]$ to determine the age for each star, but Sanders & Das (2018) did not. And we found that the parameter of $[\alpha/\text{Fe}]$ is very important to determine the stellar age, in particular for the old stellar population. Moreover, not enough young stars meet our selection criteria in the catalog of Sanders & Das (2018), e.g. only 299 stars are matched in the bin of $\tau < 0.5$ Gyr (the most left histogram). Therefore, we did not directly use the ages in this catalog, instead to re-calculate the ages with our procedure. Xiang et al. (in preparing) will discuss more about the stellar ages. Here, we just note that the age used in this study are basically consistent with ages of Sanders & Das (2018), but exist systematical differences.

4. CONCLUSION

In this Letter we reconstruct the spiral structures of $\langle v_R \rangle$ and $\langle v_\phi \rangle$ in the phase space of z - v_z using LAMOST-Gaia combined stars. We further investigate the variations of the spiral pattern with different stellar ages, and find that (1) the spirals are gradually pronounced from $\tau < 0.5$ Gyr for both $\langle v_R \rangle$ and $\langle v_\phi \rangle$, and then slowly become obscure until they almost disappear when $\tau > 6.0$ Gyr; (2) Both $\langle v_R \rangle$ and $\langle v_\phi \rangle$ in the phase space have same wiggles in the different stellar ages bins, which

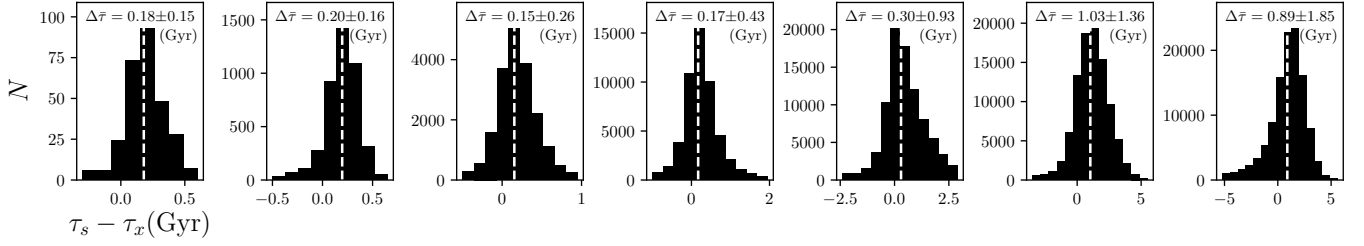


Figure 4. The histograms of age differences ($\Delta\tau = \tau_s - \tau_x$) of 416,140 cross-matched stars between our ages (τ_x) and the ages (τ_s) from [Sanders & Das \(2018\)](#). The stars are divided into seven ages bins (ages increasing from the left to right) adopted in Fig. 3. The white dashed lines mark the locations of the median age difference ($\Delta\bar{\tau}$). The stellar ages are consistent within 1σ , except in the first two young stellar bins. However, τ_s is systematically larger than τ_x by $8\% \sim 30\%$ in general.

suggest that the spirals probably have the same origin; (3) Different stellar populations respond to the perturbation by different levels of sensitivity. The stars in $\tau > 6.0$ have no spirals for both $\langle v_R \rangle$ and $\langle v_\phi \rangle$ in the phase space, probably because the old stars are kinematically hot, and almost do not respond to the perturbation. We diagnose the stellar ages used in this study, and found our ages are systematically smaller by a fraction of $8\% \sim 30\%$ than the ages of [Sanders & Das \(2018\)](#).

According to the features of the observed spirals, we infer that the vertical perturbation to the disk took place no later than 0.5 Gyr ago under the assumptions of (1) the spirals are sparked by an external perturbation, and (2) the perturbation on the ISM can be quickly dissipated, the newly born stars from the perturbed ISM do not share the general oscillations. The assumptions are possibly ideal. We need more observations or hydrodynamical simulations in high resolution to constrain the perturbation mechanism in the future.

The authors thank Prof. James Binney for his very constructive comments, and thank Chervin F. P. Laporte, Robert Grand, Hao Tian and Ling Zhu for

the helpful discussions. H.-J.T. acknowledges the National Natural Science Foundation of China (NSFC) under grants 11873034, 11503012, U1731124. C. L. acknowledges NSFC (Grant Nos. 11333003). Y. W. acknowledges NSFC (Grant No. 11403056). M.-S. Xiang acknowledges NSFC (Grant No. 11703035). This project was developed in part at the 2018 Gaia-LAMOST Sprint workshop, supported by the NSFC under grants 11333003 and 11390372. The Guo Shou Jing Telescope (the Large Sky Area Multi-Object Fiber Spectroscopic Telescope, LAMOST) is a National Major Scientific Project built by the Chinese Academy of Sciences. Funding for the project has been provided by the National Development and Reform Commission. LAMOST is operated and managed by National Astronomical Observatories, Chinese Academy of Sciences. This work has also made use of data from the European Space Agency (ESA) mission *Gaia* (<https://www.cosmos.esa.int/gaia>), processed by the *Gaia* Data Processing and Analysis Consortium (DPAC, <https://www.cosmos.esa.int/web/gaia/dpac/consortium>). Funding for the DPAC has been provided by national institutions, in particular the institutions participating in the *Gaia* Multilateral Agreement.

REFERENCES

- Antoja, T., Helmi, A., Romero-Gomez, M., et al. 2018, arXiv:1804.10196. (A18)
- Bailer-Jones, C. A. L., Rybizki, J., Fouvras, M., et al. 2018, arXiv:1804.10121B
- Binney, J., & Schönrich, R. 2018, arXiv: 1807.09819v1
- Bovy, J., Bird, J. C., García Pérez, A. E., et al. 2015, *ApJ*, 800, 83
- Cui, X.-Q., Zhao, Y.-H., Chu, Y.-Q., et al. 2012, *RAA*, 12, 1197
- Darling, K., & Widrow, L. M. 2018, arXiv:1807.11516v1
- Debatista, V. P. 2014, *MNRAS*, 443, L1
- Faure, C., Siebert, A., & Famaey, B. 2014, *MNRAS*, 440, 2564
- Kawata, D., Hunt, J. A. S., Grand, R. J. J., et al. 2014, *MNRAS*, 443, 2757
- Gaia Collaboration, Brown, A. G. A., Vallenari, A., Makarov, V. V., et al. 2016, *A&A*, 595, A2
- Gaia Collaboration: Brown, A. G. A., Vallenari, A., Makarov, V. V., et al. 2018, *A&A*, Accepted (arXiv:1804.09365G)
- Gaia Collaboration: Katz, D., Antoja, T., Romero-Gómez, M., et al. 2018, *A&A*, Accepted (arXiv:1804.09380v1)
- Gómez, F. A., Minchev, I., O’Shea, B. W., et al. 2013, *MNRAS*, 429, 159
- Grand, R. J. J., Bovy, J., Kawata, D., et al. 2015, *MNRAS*, 453, 1867

- Laporte, C. F. P., Minchev, I., Johnston, K. V., et al. 2018, arXiv:1808.0045
- Liu, X. W., Yuan, H. B., Huo, Z. Y., et al. 2014, IAUS, 298, 310L
- Liu, C., Cui, W. Y., Zhang, B., et al. 2015, RAA, 15, 1137L
- Minchev, I., Quillen, A. C., Williams, M., et al. 2009, MNRAS, 396, L56
- Monari, G., Antoja, T., & Helmi, A. 2013, arXiv:1306.2632
- Monari, G., Famaey, B., Antoja, T., et al. 2018, arXiv:1804.07767
- Quillen, A. C., Dougherty, J., Bagley, M. B., et al. 2011, MNRAS, 417, 762
- Sanders, J. L., Das, P. 2018, arXiv:1806.02324
- Siebert, A., Famaey, B., Minchev, I., et al. 2011, MNRAS, 412, 2026
- Siebert, A., Famaey, B., Binney, J., et al. 2012, MNRAS, 425, 2335
- Schönrich, R., Binney J., & Dehnen W. 2010, MNRAS, 403, 1829
- Schönrich, R. 2012 MNRAS, 427, 274
- Tian, H. J., Liu, C., Carlin, J. L., et al. 2015, ApJ, 809, 145
- Tian, H. J., Liu, C., Wan, J. C., et al. 2017, RAA, 17, 114
- Wang, H. F., López-Corredoira, M., Yanny, Carlin, J. L., et al. 2018, MNRAS, 750, L41
- Wang, H. F., Liu, C., Xu, Y., et al. 2018, MNRAS, 478, 3367
- Widrow, L. M., Gardner, S., Yanny, B., Dodelson, S., & Chen, H.-Y. 2012, ApJL, 750, L41
- Worthey, G., Faber, S. M., Gonzalez, J. J., & Burstein, D. 1994, ApJS, 94, 687
- Wu, Y., L., A-Li, Li, Hai-Ning, et al. 2011a, RAA, 11, 924
- Wu, Y., Singh, H.P., Prugniel, P., et al. 2011b, A&A, 525, 71
- Wu, Y., Du, B., et al. 2014, IAUS, 306, 340W
- Xiang, M. S., Liu, X. W., Yuan, H. B. et al. 2015, MNRAS, 448, 822
- Xiang, M. S., Liu, X. W., Shi, J. R., et al. 2017, ApJS, 232, 2
- Xiang, M. S., Shi, J. R., Liu, X. W., et al. 2018, ApJS, Accepted (arXiv:1807.04592)
- Xu, Y., Newberg, H. J., Carlin, J. L., et al. 2015, ApJ, 801, 105
- Zhao, G., Zhao, Y. H., Chu, Y. Q., et al. 2012, RAA, 12, 723